Decoding Motor Imagery of three-dimensional Random Movements Using Electrocorticographic Signals in Acute Training Setting

Chun Kee Chung (chungc@snu.ac.kr)
Seoul National University College of Natural Sciences
Yu Jin Yang
Seoul National University College of Natural Sciences
Seokyun Ryun
Seoul National University Medical Research Center
June Sic Kim
Seoul National University College of Natural Sciences

Research Article

Keywords: Brain-Machine Interface, Decoding, Electrocorticography, Motor execution, Motor imagery

Posted Date: March 8th, 2022

DOI: https://doi.org/10.21203/rs.3.rs-1402386/v1

Abstract

Background: Decoding movement-related signals from widespread brain areas may be advantageous given that diverse brain areas are activated for complex movements and imagined movements. Electrocorticography (ECoG) is a beneficial option in that it covers wide brain areas with a high signal-to-noise ratio. Here, we used ECoG to decode human reach-and-grasp movements and imagined movements.

Method: Twenty-two epileptic patients with intracranial electrodes were asked to execute and imagine reach-and-grasp movements toward random targets with training periods of 8.2± 3.4 days. A multiple linear regression algorithm was used to estimate the offline prediction of the movement and imagined movement trajectories.

Result: The three-dimensional reaching trajectories were decoded in motor execution (ME) and motor imagery (MI) tasks. The mean correlation coefficients for the x-axis, y-axis, and z-axis were correspondingly 0.5, 0.53, and 0.51 for the ME and 0.37, 0.19, and 0.28 for the MI.

Conclusion: MI could be decoded in subjects who were acutely trained with acceptable performance when given a random target presentation task. ECoG brain-machine interface (BMI) given its wide coverage may be practical for decoding movements with multiple degrees of freedom in humans.

Introduction

In the 1970s, it was revealed through single-cell recordings of the monkey primary motor coetex (M1) that certain cells in the M1 fire in a preferred direction [1]. This has evolved into a brain-machine interface (BMI) that connects neural signals to external devices. Several signal platforms can be used as input signals for BMIs in a clinical setting. Microelectrode arrays (MEAs) were used in monkeys [2] and in paralyzed patients [3-5], as such arrays are known to convey large amounts of information. However, these signals were not from diverse cortical areas and used only selected areas (e.g., M1, posterior parietal cortex). Small, high-impedance recordings make penetrating electrodes vulnerable to signal degradation due to encapsulation, resulting in device failure. These are crucial obstacles that currently prohibit their clinical use in humans. Recently, signals linked to macro-scale oscillation activity, such as electrocorticography (ECoG), have emerged as BMI candidate signals. ECoG, with long-lasting signal quality, can record local activities from multiple neurons and does not require the penetration of brain tissue. Thus, ECoG recordings from the cortical surface could be a powerful and practical alternative to current BMI recording methods.

However, because the people who most need BMI are disabled and cannot move (e.g., spinal cord injury, locked-in syndrome), they use BMI using motor imagery (MI), in which a person imagines a body part moving without corresponding motor output [6]. In 1995, MI was conceptualized as a type of movement [6]. Since then, numerous neurophysiological studies have reported MI activities. However, the activities

during MI have been found to be less intense than those of ME [7,8]. A magnetoencephalography (MEG) study found low-frequency activity with MI [7]. With ECoG in MI, a similar neural pattern was detected on the sensorimotor cortex, reminiscent of ME [8,9]. Moreover, functional magnetic resonance imaging (MRI) studies revealed that the superficial layer of M1 was activated in both ME and MI conditions, while the deep layer of M1 was only activated in the ME condition [10]. Hence, MI could be decoded like ME signals, though these outcomes are less active and limited.

Numerous studies have attempted to decode MI in BMI in various ways. First, in MEA studies, researchers used the neural activity from the M1, not from diverse brain activities, similar to how actual movements are decoded [3,4]. Moreover, most studies which used ECoG signals mainly decoded simple movements, such as two-dimensional control using MI signals [11-14], and classified two classes of MI [15]. Except for one study [16], researchers have not decoded complex movements of MI such as three-dimensional arm trajectories using ECoG signals. We intended to decode these types of three-dimensional MI signals with a regression method. Moreover, because diverse brain areas are activated during MI [17-20], we attempted to incorporate features from wide cortical areas that may be useful for movement decoding. Also, to address the gap between ME and MI, we asked the patients who were subjects here to perform ME and MI in turn to facilitate their somatosensory imagination, also known as kinesthetic motor imagery (KMI).

The present study aimed to examine whether using ECoG signals from the widespread motor-related areas would be useful for three-dimensional arm movements and for movement imagery decoding and whether the decoding performance of this method is comparable to that of population neural activities. Therefore, we hypothesized that MI could be decoded identically to ME decoding, even if underperforming ME.

Methods

Patients

We recruited medically intractable epilepsy patients who needed intracranial electrodes for localizing the seizure onset zone and for functional mapping. The experiment involved a total of 22 patients (11 females; age range, 21-49 years). However, four datasets were excluded from the analysis due to technical issues when recording the neural signals. Also, one of the remaining subjects failed to perform ME properly due to arm weakness, causing the data from this additional patient to be excluded (Figure 1). Subdural ECoG electrodes were used as strips and/or grids (Ad-tech Medical Instrument, Racine, WI, USA) and high-density grids (PMT Corporation, Chanhassen, MN, USA). The locations of the electrodes were purely determined for clinical purposes and are illustrated in Figure 2. ECoG electrodes were implanted for 8.2 ± .4 days and the experiment were performed once, except for S1, S4, S8, and S10, who participated twice. The average task time for the experiment was 42.3±7.5 minutes. For each patient, preoperative MR images and postoperative computed tomgraphy (CT) images were acquired. Co-registrations between

preoperative MRI and postoperative CT images for localization of ECoG electrodes were performed semi-automatically using CURRY software (version 7.0; Compumedics Neuroscan).

This study was performed under the Declaration of Helsinki and was approved by the Institutional Review Board (IRB) of Seoul National University Hospital (1403-093-566). All patients provided written informed consent before participating. Table 1 contains demographic and clinical information for all 17 patients. All of them were right-handed, and all electrode arrays were located in the unilateral hemisphere.

Instructions and Tasks

The patients performed three-dimensional center-out reach-and-grasp tasks. Patients moved their arm contralateral to the implantation sites. The task comprises ME and MI. Each trial consisted of a cue, reaching, grasping, and return periods. Before the task, the patients had to position in the initial status, referring to the positioning of the patient's hand in front of their abdomen (see Figures 3A and 3B). In the cue period, the experimenter presented a target ball in one of the four directions to the patients. The position of the target was the corner of a square, and the center of the square was the position of the hand in the initial status. Patients were instructed to move their arm as far as possible toward the target. This was done to elicit the greatest difference in movement that the subject could make with his/her arms. The target position was slightly different despite the fact that it was in the same quadrant because the experimenter presented the target at every trial. After the cue period, the patient reached the target ball and when they completely reached the target, they grasped around the target. This occurred because the experimenter presented the target outside of the range of where the patient could reach and grasp while sitting. They then returned to their initial status in the grasped state. They released their grasp when they completely reached the initial status (Figure 3C). After the movement task, the patients performed an imagery task. From the initial status, after the experimenter presented the target ball, the patients were asked to perform kinesthetic imagery by feeling the somatosensations of the prior movement. In the imagery task, the target direction was identical to that in the previous execution task because motor imagery is difficult to perform without any prior sensory stimuli [21,22]. The four directions of the target were presented in a random order. A block consists of an execution trial and an imagery trial. One session was composed of several blocks. The number of trials for each subject is illustrated in Table 1. For subject 1 and subject 3, the ME task was performed more frequently. All experiments were recorded on video to monitor the task performance of the patients.

Electrophysiological Recordings and Preprocessing

ECoG data were recorded with a 128-channel amplifier system (Neuroscan synamps2, Compumedics, Abbotsford, Victoria, Australia). The movements of the arm and hand were tracked by a motion-capture system with an active optical marker. Six markers were fixed to the patients' arms and hands, contralateral to the implanted hemisphere (3D investigator, Northern Digital Inc., Waterloo, Ontario, Canada) during the neural signal recording process. The sampling frequency was 2,000Hz for the ECoG.

Kinematic data were sampled at 100Hz and were synchronized with ECoG signals. We delivered a 5 V input simultaneously to all devices before starting the sessions to synchronize the ECoG amplifier and the motion tracker (i.e., through the transistor-transistor logic (TTL) port of the ECoG amplifier and the external trigger port of the 3D investigator amplifier). In the imagery trials, because it was impossible to find the exact onset time, the experimenter noted only the target presentation time. The common average reference (CAR) was used to re-reference the recorded data. To remove power noise at 60 Hz and the related harmonics, the signals were notch-filtered with a finite impulse response (FIR) filter using the eegfilt function in the EEGLAB toolbox [23]. We used splitters and Y-shaped connectors, allowing us to send signal copies of voltage traces to the clinical amplifier so as not to interrupt the clinical monitoring process.

Decoding Algorithms

We used a simple regression algorithm from the published literature [24]. Briefly, low-frequency ECoG signals (0.5-8 Hz) were used to predict the movement velocity. Velocity predictions were selected because it is known that velocity provides higher performance than position and acceleration [25]. We chose a low frequency because the low frequency band shows the highest performance [26]. We analyzed low frequency bands as in our previous papers [24,27]. The signals resampled at an interval of 12ms were used to estimate the current movement velocity [28]. We also estimated the current movement velocity using the current time point plus the corresponding 20 previous time points (for a total of 21 points) corresponding to 252ms intervals [28]. These 21 points for all channels were used as features; also, the x, y, and z velocities of the movements were estimated using a multiple linear regression method, as follows:

$$x(t) = \sum_{i=1}^{n}\sum_{j=0}^{m} W_{ij}^{x} \times S_i(t-j) + W_0^{x}$$

$$y(t) = \sum_{i=1}^{n}\sum_{j=0}^{m} W_{ij}^{y} \times S_i(t-j) + W_0^{y}$$

$$z(t) = \sum_{i=1}^{n}\sum_{j=0}^{m} W_{ij}^{z} \times S_i(t-j) + W_0^{z}$$

where $x(t)$, $y(t)$ and $z(t)$ are the predicted movement (or imagery) velocities at time t. W_{ij}^{x}, W_{ij}^{y} and W_{ij}^{z} are the weight value matrices, which are obtained using the regression methods. S_i is the ECoG signal of channel i. The parameter n denotes the number of channels. The parameter m denotes the number of data points before time t, which determines the number of previous data points used to predict the current velocities $x(t)$, $y(t)$, and $z(t)$. The parameter j refers to the time lag, and W_0 is a constant used to compensate for errors. The parameters W_{ij} and W_0 were obtained from training by means of multiple linear regression.

Evaluation of the prediction performance

We calculated the correlation coefficients using five-fold cross-validation. This method separates the data into four-fifths for training and one-fifth for testing [29]. Therefore, five combinations of training and testing data were available. Weight parameters were obtained using the training data, and the correlation coefficients of the estimations were evaluated using the testing data by calculating the Pearson's correlation coefficients (r) between the real and predicted movement trajectories for each cross-validation fold. The correlation coefficients were averaged throughout the cross-validation folds.

Trajectories of Arm Movements

To visualize the trajectories of the real and predicted arm movements, we compute the position by integrating the actual velocity and the predicted velocity, respectively. Given that the motion tracker measures the position data, we differentiated the position data to calculate the velocity. The initial status was set to zero when visualizing the results. We illustrated the trajectories only during reaching

movements. Because the patients did not move under the MI condition, the averaged trajectory of ME was used as the MI trajectory in each case when training the weights for the MI condition (Figure 4C).

Results

Decoding Performance

The mean Pearson's correlation coefficients between the real and predicted trajectories (ME and MI, respectively) are shown in Table 2. The mean correlation coefficients for the x-axis, y-axis, and z-axis for 17 subjects were correspondingly 0.5, 0.53, and 0.51 for ME and 0.37, 0.19, and 0.28 for MI. The average correlation coefficients of the five subjects with the highest correlations were likewise 0.59, 0.67, and 0.63 for ME and 0.49, 0.38, and 0.49 for MI.

The arm trajectory is successfully decoded from the widespread cortical areas. This indicates that in addition to the primary motor cortex, the movement information is encoded in other cortical areas. The performance was varied between ME and MI. Figure 4 shows the data from subject 8, whose decoding performance of MI was highest among all subjects. Figures 4A and 4B show the ME and predicted ME trajectories, respectively. Figures 4C and 4D likewise show the averaged ME trajectory used to train the MI data and the predicted MI trajectory.

Discussion

In this study, we asked patients undergoing ECoG recording to move their natural arm and to perform imaginary movements in turn. The correlation coefficients between the real and predicted ME trajectories were comparable to those in recent studies which decoded three-dimensional arm movements (average Pearson's correlation coefficients for velocity were 0.45, 0.35 and 0.42 in five patients) [30]. In addition, the decoding performance of MI is comparable to the results after the training of tetraplegic patients to use attempt movement-based BMI for one to two years with wireless ECoG implantation [16].

It is generally thought that ECoG signals are not sufficient to decode MI owing to their low level of informativeness compared to MEAs. However, we demonstrated that ECoG signals can be used to predict three-dimensional reaching movements and movement imagery with a high correlation coefficient using simple regression algorithms. This may have been possible due to the benefit of collecting movement-related signals from broader brain areas, which is important for complex movements. Diverse brain regions are involved in skilled movements, such as reaching and grasping, as skilled movements require multiple cognitive functions, such as generating potential action plans, selecting from among them, and converting the plans into detailed motor commands [31].

We designed a task paradigm similar to that in our previous paper [32]. We used a block design because movement imagery is difficult without any preceding practical task [21]. We also expect that the prior execution tended to prime the imagery sequences and to elicit somatosensations easily when performing

MI [33]. Also, our previous paper showed significant Pearson's correlation coefficients ($p < 0.01$) between the connectivity of ME and KMI [32], suggesting that ME and MI share similar brain networks.

We found that neural signals during ME and MI are successfully decoded through ECoG signals (Table 2). High performance of ME and MI decoding could be established by large-scale neural signal acquisitions. Also, we trained our subjects in four directions, but the target positions in each direction differed slightly. Therefore, we can argue that we trained subjects with the paradigm of random target tasks and successfully decoded these types of neural activities. It could thus be further presumed that the subjects may have used their natural movements easily with this type of BMI.

Some subjects showed high decoding performance in ME, while MI showed low performance (e.g., Subject 3). Decoding of an actual movement is primarily governed by the movement-related information from the predestined location of the electrodes. Therefore, if the patient's ME performance is low, it is reasonable to conclude that there may be little movement-related information from the electrodes. However, if the subject's decoding performance in ME is high but low in MI, this may not be due to low-movement-related information per se, but to other reasons. One plausible reason is BMI illiteracy [34]. More training time, additional training methods, and feedback are needed to train people with BMI illiteracy. However, the training time is limited here due to the clinical monitoring period. Therefore, more research is needed to train people who are not adept with regard to their use of these types of BMIs, and it is expected that the correlation coefficients between the real and predicted trajectories would increase through sufficient training.

Although our results exhibited high performance, the study has limitations in that we made only offline predictions. For more practical meaning, closed-loop BMI should be implemented, as feedback information is crucial for learning MI. Future research should provide feedback information to the subjects when training MI. The second limitation of the present study is related to the variability of performance outcomes. For example, the correlation coefficients of subject 5 in the ME condition were 0.40, 0.19, 0.30 for the x, y, and z axis, respectively, representing the lowest performance on ME among all subjects, while the highest performance outcomes on ME were 0.63, 0.67, and 0.73 for x, y, and z axis respectively, by subject 8. The locations of the electrodes can be a cause of the performance variability. The electrode location of subject 5 was mainly in the temporal lobe, with 12 electrodes, the lowest number of electrodes among the subjects (average number of electrodes for the 17 subjects = 34±14). However, subject 8 had 54 electrodes in the temporal, parietal and occipital cortexes (37, 13 and 4, respectively). This may explain the high performance in this case, as the electrode number is crucially related to the decoding performance [35]. The low performance of MI could be the reason for the BMI illiteracy. However, the high performance of MI by subject 8, as illustrated in Figure 4, was exceptional and thus can infer that subject 8 is an excellent participant in the MI control task.

Conclusion

In this study, we show that the decoding performance of MI, which performed an average of 1.24±0.42 experiments per subject, was acceptable. The acceptable performance of ECoG-based BMI can be attributed to the fact that subjects performed MI after actual movements, which could facilitate kinesthetic sensation. These findings imply that patients with tetraplegia can use BMI by using MI with multiple degrees of freedom. This result will open up new vistas on ME and MI in the research on ECoG BMI.

Declarations

Authors' contributions

Y. J. Yang: analysis of data, acquisition of data, writing of original draft; S. R. Ryun: supervision, writing - review & editing; J. S. Kim: Supervision, writing - review & editing; C. K. Chung: funding acquisition, supervision, design and conceptualization, writing - review & editing.

Acknowledgements

Thanks to H. Yeom for providing the helpful materials and advice, and to S. Kim for all of the valuable comments.

Author Disclosure Statement

The authors declare that no competing financial interests exist.

Data availability

The datasets used and/or analysed during the current study available from the corresponding author on reasonable request.

References

1. Georgopoulos, A. P., Kalaska, J. F., Caminiti, R. & Massey, J. T. On the Relations between the Direction of Two-Dimensional Arm Movements and Cell Discharge in Primate Motor Cortex. *J Neurosci* **2**, 1527-1537 (1982).
2. Velliste, M., Perel, S., Spalding, M. C., Whitford, A. S. & Schwartz, A. B. Cortical control of a prosthetic arm for self-feeding. *Nature* **453**, 1098-1101 (2008).
3. Hochberg, L. R.*et al.* Reach and grasp by people with tetraplegia using a neurally controlled robotic arm. *Nature* **485**, 372-U121 (2012).

4. Collinger, J. L.*et al.* High-performance neuroprosthetic control by an individual with tetraplegia. *Lancet* **381**, 557-564, doi:10.1016/S0140-6736(12)61816-9 (2013).
5. Aflalo, T.*et al.* Decoding motor imagery from the posterior parietal cortex of a tetraplegic human. *Science* **348**, 906-910 (2015).
6. Jeannerod, M. Mental-Imagery in the Motor Context. *Neuropsychologia* **33**, 1419-1432, doi:Doi 10.1016/0028-3932(95)00073-C (1995).
7. Kraeutner, S., Gionfriddo, A., Bardouille, T. & Boe, S. Motor imagery-based brain activity parallels that of motor execution: evidence from magnetic source imaging of cortical oscillations. *Brain Res* **1588**, 81-91, doi:10.1016/j.brainres.2014.09.001 (2014).
8. Miller, K. J.*et al.* Cortical activity during motor execution, motor imagery, and imagery-based online feedback. *Proc Natl Acad Sci U S A* **107**, 4430-4435, doi:10.1073/pnas.0913697107 (2010).
9. Miller, K. J.*et al.* Spectral changes in cortical surface potentials during motor movement. *J Neurosci* **27**, 2424-2432, doi:10.1523/JNEUROSCI.3886-06.2007 (2007).
10. Persichetti, A. S., Avery, J. A., Huber, L., Merriam, E. P. & Martin, A. Layer-Specific Contributions to Imagined and Executed Hand Movements in Human Primary Motor Cortex. *Curr Biol* **30**, 1721-+, doi:10.1016/j.cub.2020.02.046 (2020).
11. Leuthardt, E. C., Schalk, G., Wolpaw, J. R., Ojemann, J. G. & Moran, D. W. A brain-computer interface using electrocorticographic signals in humans. *Journal of Neural Engineering* **1**, 63-71 (2004).
12. Schalk, G.*et al.* Decoding two-dimensional movement trajectories using electrocorticographic signals in humans. *Journal of Neural Engineering* **4**, 264-275 (2007).
13. Schalk, G.*et al.* Two-dimensional movement control using electrocorticographic signals in humans. *Journal of Neural Engineering* **5**, 75-84, doi:10.1088/1741-2560/5/1/008 (2008).
14. Felton, E. A., Wilson, J. A., Williams, J. C. & Garell, P. C. Electrocorticographically controlled brain-computer interfaces using motor and sensory imagery in patients with temporary subdural electrode implants - Report of four cases. *J Neurosurg* **106**, 495-500 (2007).
15. Rashid, M.*et al.* Electrocorticography based motor imagery movements classification using long short-term memory (LSTM) based on deep learning approach. *Sn Appl Sci* **2**, doi:ARTN 21110.1007/s42452-020-2023-x (2020).
16. Benabid, A. L.*et al.* An exoskeleton controlled by an epidural wireless brain-machine interface in a tetraplegic patient: a proof-of-concept demonstration. *Lancet Neurol* **18**, 1112-1122, doi:10.1016/S1474-4422(19)30321-7 (2019).
17. Lacourse, M. G., Orr, E. L. R., Cramer, S. C. & Cohen, M. J. Brain activation during execution and motor imagery of novel and skilled sequential hand movements. *Neuroimage* **27**, 505-519, doi:10.1016/j.neuroimage.2005.04.025 (2005).
18. Lotze, M.*et al.* Activation of cortical and cerebellar motor areas during executed and imagined hand movements: An fMRI study. *J Cognitive Neurosci* **11**, 491-501 (1999).

19. Jeannerod, M. Neural simulation of action: A unifying mechanism for motor cognition. *Neuroimage* **14**, S103-S109, doi:10.1006/nimg.2001.0832 (2001).
20. Hetu, S.*et al.* The neural network of motor imagery: an ALE meta-analysis. *Neurosci Biobehav Rev* **37**, 930-949, doi:10.1016/j.neubiorev.2013.03.017 (2013).
21. Papaxanthis, C., Pozzo, T., Skoura, X. & Schieppati, M. Does order and timing in performance of imagined and actual movements affect the motor imagery process? The duration of walking and writing task. *Behav Brain Res* **134**, 209-215, doi:Pii S0166-4328(02)00030-XDoi 10.1016/S0166-4328(02)00030-X (2002).
22. Sheahan, H. R., Ingram, J. N., Zalalyte, G. M. & Wolpert, D. M. Imagery of movements immediately following performance allows learning of motor skills that interfere. *Sci Rep-Uk* **8** (2018).
23. Delorme, A. & Makeig, S. EEGLAB: an open source toolbox for analysis of single-trial EEG dynamics including independent component analysis. *J Neurosci Meth* **134**, 9-21 (2004).
24. Yeom, H. G., Kim, J. S. & Chung, C. K. Estimation of the velocity and trajectory of three-dimensional reaching movements from non-invasive magnetoencephalography signals. *J Neural Eng* **10**, 026006, doi:10.1088/1741-2560/10/2/026006 (2013).
25. Kim, S. P., Simeral, J. D., Hochberg, L. R., Donoghue, J. P. & Black, M. J. Neural control of computer cursor velocity by decoding motor cortical spiking activity in humans with tetraplegia. *Journal of Neural Engineering* **5**, 455-476 (2008).
26. Hammer, J.*et al.* The role of ECoG magnitude and phase in decoding position, velocity, and acceleration during continuous motor behavior. *Front Neurosci-Switz* **7** (2013).
27. Yeom, H. G., Kim, J. S. & Chung, C. K. LSTM Improves Accuracy of Reaching Trajectory Prediction From Magnetoencephalography Signals. *Ieee Access* **8**, 20146-20150 (2020).
28. Toda, A., Imamizu, H., Kawato, M. & Sato, M. A. Reconstruction of two-dimensional movement trajectories from selected magnetoencephalography cortical currents by combined sparse Bayesian methods. *Neuroimage* **54**, 892-905 (2011).
29. Fruitet, J., McFarland, D. J. & Wolpaw, J. R. A comparison of regression techniques for a two-dimensional sensorimotor rhythm-based brain-computer interface. *Journal of Neural Engineering* **7** (2010).
30. Bundy, D. T., Pahwa, M., Szrama, N. & Leuthardt, E. C. Decoding three-dimensional reaching movements using electrocorticographic signals in humans. *Journal of Neural Engineering* **13**, doi:Artn 02602110.1088/1741-2560/13/2/026021 (2016).
31. Cui, H. & Andersen, R. A. Different Representations of Potential and Selected Motor Plans by Distinct Parietal Areas. *J Neurosci* **31**, 18130-18136 (2011).
32. Yang, Y. J., Jeon, E. J., Kim, J. S. & Chung, C. K. Characterization of kinesthetic motor imagery compared with visual motor imageries. *Sci Rep-Uk* **11** (2021).
33. Neuper, C., Scherer, R., Reiner, M. & Pfurtscheller, G. Imagery of motor actions: Differential effects of kinesthetic and visual-motor mode of imagery in single-trial EEG. *Cognitive Brain Res* **25**, 668-677 (2005).

34. Vidaurre, C. & Blankertz, B. Towards a cure for BCI illiteracy. *Brain Topogr* **23**, 194-198, doi:10.1007/s10548-009-0121-6 (2010).
35. Sannelli, C.*et al.* On optimal channel configurations for SMR-based brain-computer interfaces. *Brain Topogr* **23**, 186-193, doi:10.1007/s10548-010-0135-0 (2010).

Tables

Table 1

CHARACTERISTICS OF THE SUBJECTS

	Diagnosis	Electrode location	Number of electrodes	Sex/Age	Trial number (ME)/(MI)
S1	TLE	Frontal Lobe	5	M/41	171/56
		Temporal Lobe	12		
		Parietal Lobe	15		
S2	FLE	Frontal Lobe	25	M/29	126/126
		Temporal Lobe	4		
		Parietal Lobe	3		
S3	TOLE	Frontal Lobe	10	F/32	123/70
		Temporal Lobe	4		
		Parietal Lobe	4		
		Occipital Lobe	4		
S4	FLE	Frontal Lobe	14	F/22	286/286
		Temporal Lobe	25		
		Parietal Lobe	17		
S5	Medial-TLE	Frontal Lobe	2	F/29	169/169
		Temporal Lobe	10		
S6	TLE	Frontal Lobe	10	F/23	166/166
		Temporal Lobe	33		
		Occipital Lobe	1		
S7	FLE	Temporal Lobe	10	M/24	172/172
		Parietal Lobe	29		
		Occipital Lobe	23		
S8	TLE	Temporal Lobe	37	M/28	227/227
		Parietal Lobe	13		
		Occipital Lobe	4		
S9	TLE	Frontal Lobe	9	F/22	159/159
		Temporal Lobe	11		
		Parietal Lobe	4		
S10	TLE	Frontal Lobe	3	F/27	237/237

		Temporal Lobe	9		
		Parietal Lobe	6		
S11	TLE	Frontal Lobe	13	F/36	158/158
		Temporal Lobe	18		
		Parietal Lobe	11		
S12	TLE	Frontal Lobe	7	M/21	148/148
		Temporal Lobe	12		
		Parietal Lobe	5		
S13	TLE	Frontal Lobe	15	F/29	84/84
		Temporal Lobe	28		
		Parietal Lobe	7		
S14	TLE	Frontal Lobe	11	M/58	143/143
		Temporal Lobe	12		
		Parietal Lobe	16		
		Occipital Lobe	1		
S15	TLE	Temporal Lobe	17	M/49	164/164
		Parietal Lobe	9		
		Occipital Lobe	2		
S16	TLE	Frontal Lobe	1	M/36	152/152
		Temporal Lobe	8		
		Parietal Lobe	5		
		Occipital Lobe	2		
S17	TLE	Frontal Lobe	7	F/31	173/173
		Temporal Lobe	13		
		Parietal Lobe	6		

TLE, temporal lobe epilepsy; TOLE, temporo-occipital lobe epilepsy; FLE, frontal lobe epilepsy; F, Female; M, Male;

Table 2
TRAJECTORY CORRELATION COEFFICIENTS (PEARSON'S R) OF REAL AND PREDICTED ARM TRAJECTORIES.

	Corr(ME)			Corr(MI)		
	x	y	z	x	y	z
S1	0.60	0.51	0.46	0.67	0.06	0.31
S2	0.35	0.21	0.32	0.08	0.10	0.12
S3	0.42	0.72	0.54	0.12	0.19	0.16
S4	0.57	0.72	0.56	0.54	0.42	0.57
S5	0.40	0.19	0.30	0.26	0.07	0.04
S6	0.65	0.71	0.58	0.50	0.37	0.45
S7	0.53	0.55	0.55	0.21	0.08	0.09
S8	0.63	0.67	0.73	0.63	0.63	0.68
S9	0.63	0.67	0.66	0.53	0.34	0.56
S10	0.37	0.63	0.57	0.30	0.36	0.46
S11	0.47	0.57	0.59	0.25	0.13	0.18
S12	0.72	0.49	0.44	0.41	0.05	0.15
S13	0.55	0.44	0.47	0.39	-0.13	-0.10
S14	0.38	0.55	0.63	0.18	0.10	0.25
S15	0.39	0.44	0.49	0.32	0.32	0.32
S16	0.41	0.48	0.45	0.46	-0.05	0.23
S17	0.48	0.48	0.34	0.42	0.24	0.21

Figures

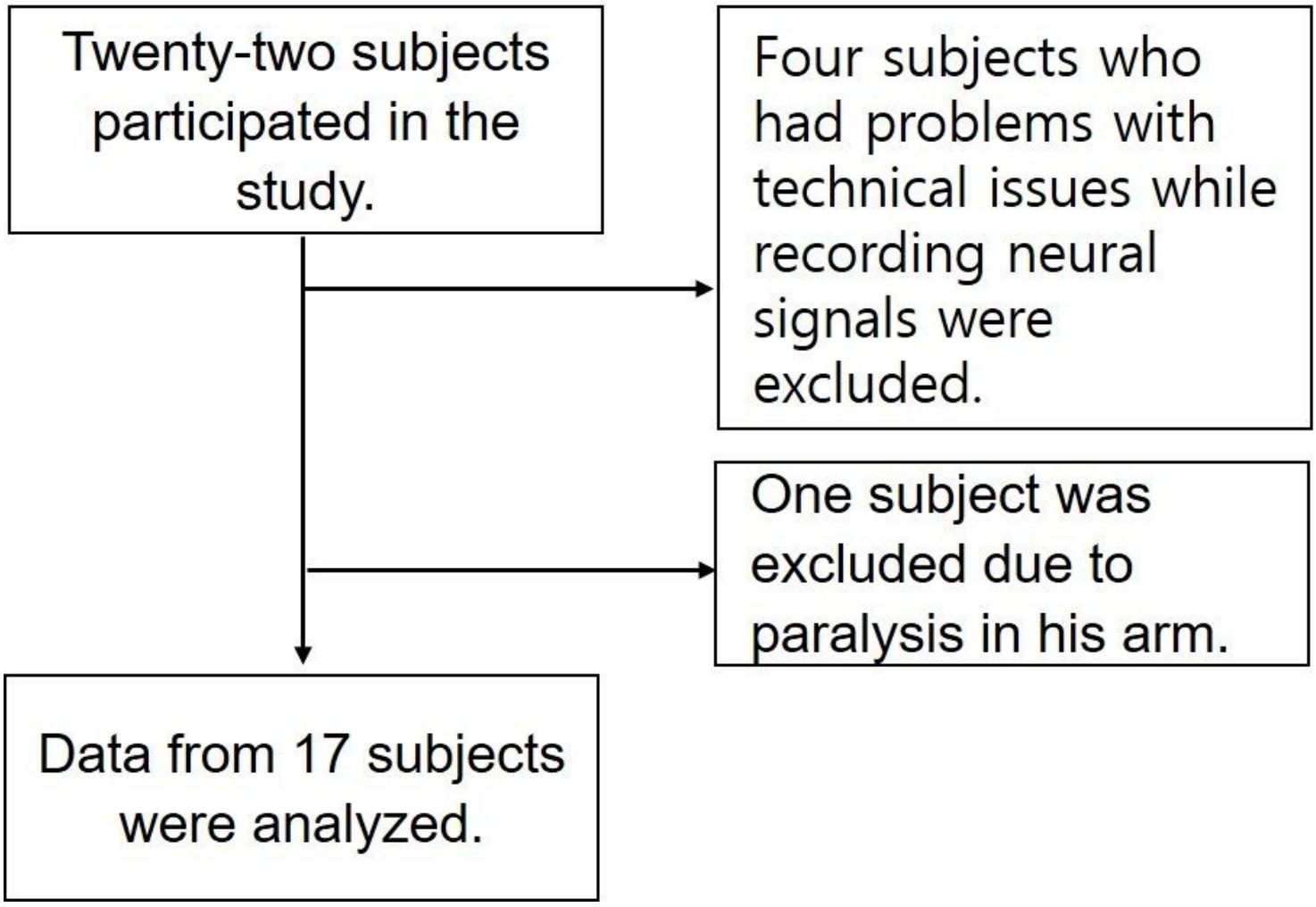

Figure 1

Subject recruitment flow diagram

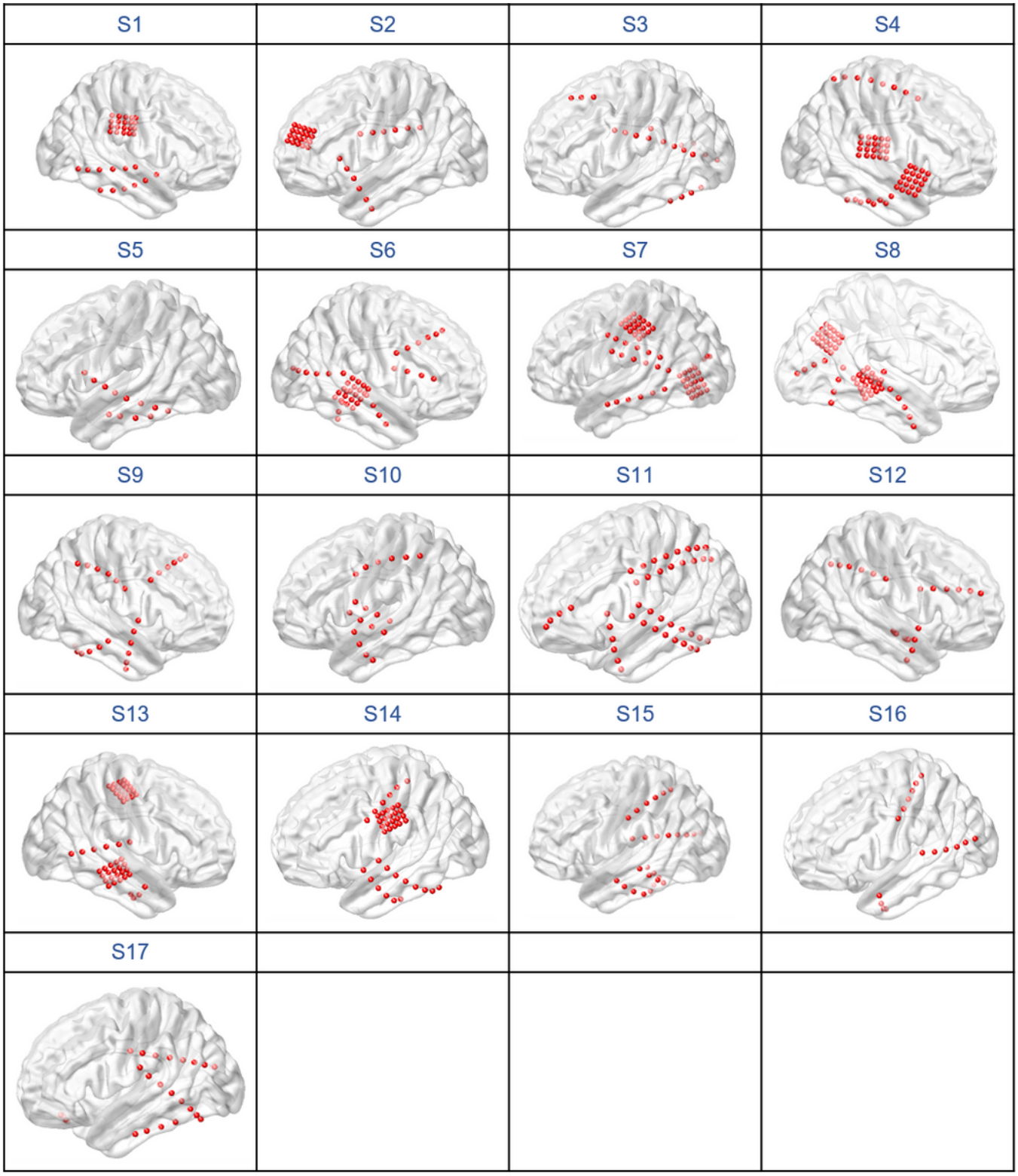

Figure 2

Locations of ECoG electrodes in all subjects

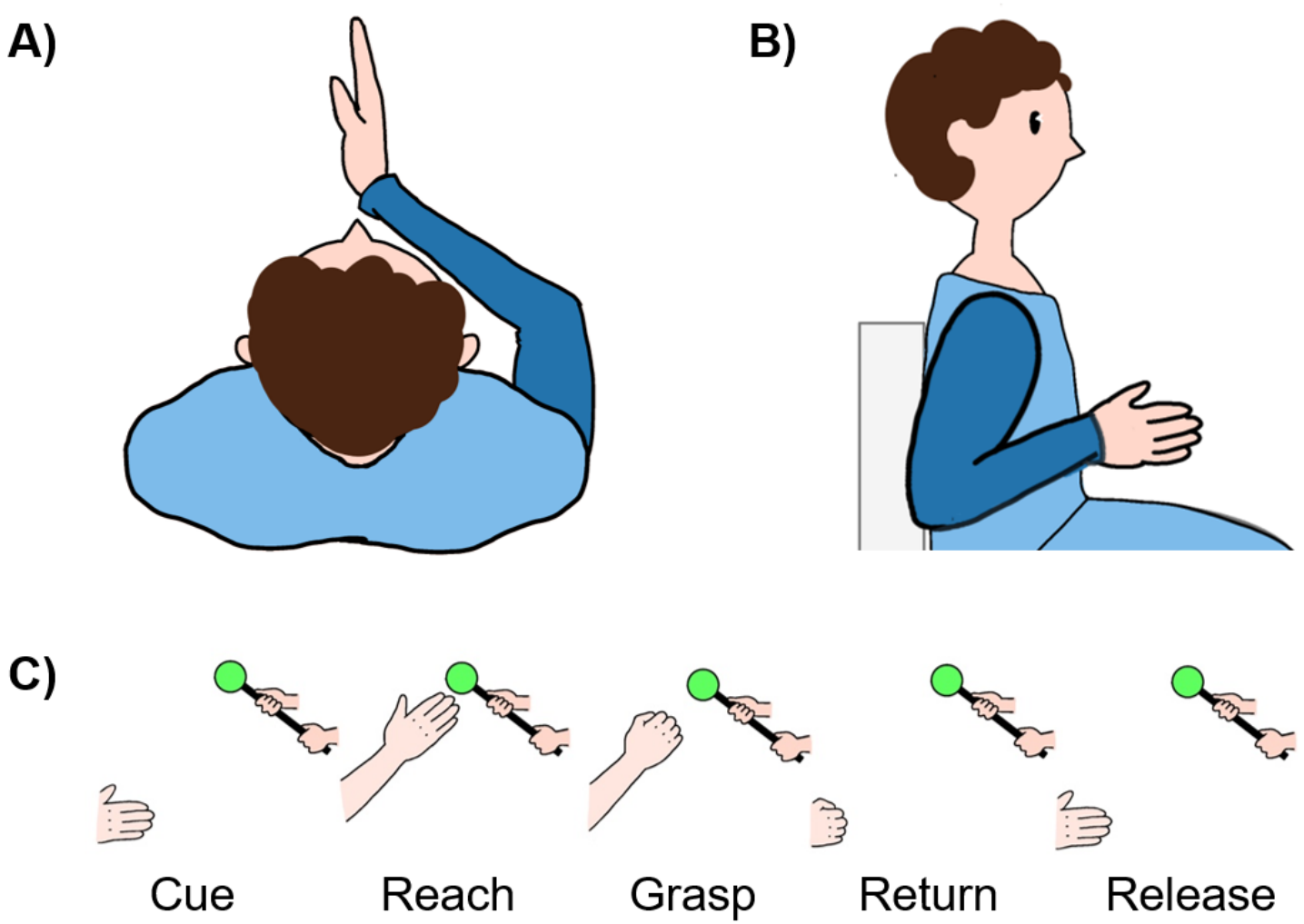

Figure 3

An example of the initial status from this study: (A) top-view of the initial status, (B) lateral view of the inietial status, and (C) graphical illustration of the task design

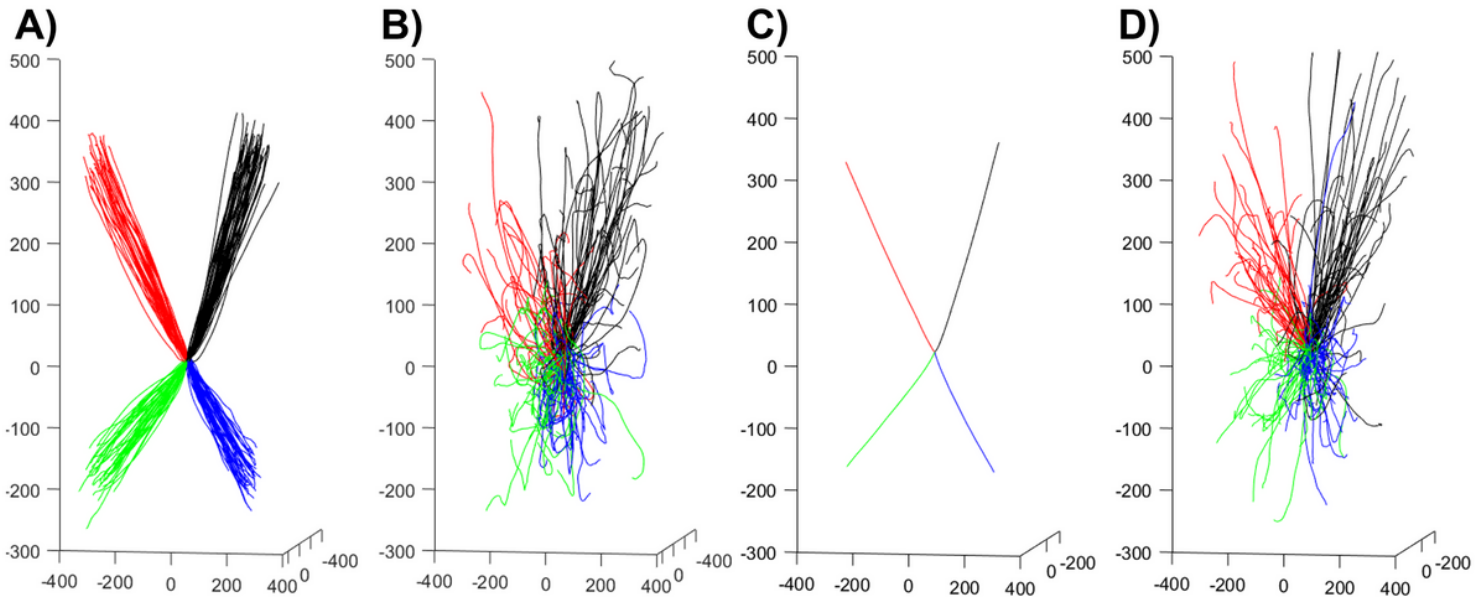

Figure 4

Real and predicted arm trajectories of subject 8, each color indicates one of four different directions. A) trajectory of ME, B) predicted ME trajectory, C) average of the ME trajectory used for training MI data, and D) predicted MI trajectory